Available online at www.sciencedirect.com

ScienceDirect

journal homepage: www.elsevier.com/locate/he

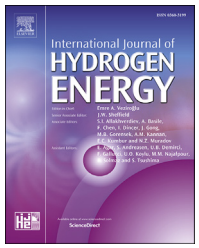

Ex situ measurement and modelling of crack propagation in fuel cell membranes under mechanical fatigue loading

Y. Singh, R.M.H. Khorasany, A. Sadeghi Alavijeh, E. Kjeang*, G.G. Wang, R.K.N.D. Rajapakse

Fuel Cell Research Lab (FCReL), School of Mechatronic Systems Engineering, Simon Fraser University, 250-13450 102 Avenue, Surrey, BC, V3T 0A3, Canada

ARTICLE INFO

Article history:
Received 15 February 2017
Received in revised form
4 June 2017
Accepted 19 June 2017
Available online 11 July 2017

Keywords:
Fuel cell
Durability
Crack propagation
Paris law
Fracture
Elasto-viscoplasticity

ABSTRACT

Fatigue-induced membrane fracture due to dynamic stresses is an important lifetime-limiting failure mode in automotive fuel cell applications. Here, a series of *ex situ* experiments are first conducted to measure the rate of crack growth in Nafion NRE211 membranes for a range of stress, temperature (23–70 °C), and relative humidity (50–90%) conditions relevant to automotive fuel cell operation. The crack growth rate is found to be ~1–10 nm per load cycle and strongly depends on the stress intensity: the rate increases by an order of magnitude for a mere 10–30% increase in stress, which suggests that improved stress uniformity and avoidance of high stress points is important for durability. Moreover, the sensitivity to applied stress doubles from room conditions to fuel cell conditions, where the temperature has 2–3x stronger impact on the fracture propagation than the relative humidity. Microstructural analysis indicates that plastic deformation (60% localized thinning) at the crack tip accompanies crack growth. A semi-analytical model based on Paris law is then developed to simulate crack growth as a function of cyclic loading. The model incorporates elastic-viscoplastic mechanical behaviour of ionomer membranes and provides crack growth predictions in agreement with *ex situ* data up to 100% strain.

Introduction

Fuel cell engines hold great promise as potential power sources for automotive applications in the 21st century. They offer a clean, noise-free, efficient, and lightweight solution compared to the incumbent heat engines; however, their inferior durability puts them at an economic disadvantage that consequently impedes their large-scale commercial adoption. The durability requirements for an automobile must be met under transient power cycle operation, many start/stops, and over a range of operating temperatures [1]. In a fuel cell, such varying operating conditions have been found to cause excessive degradation which negatively impacts their performance and limits their operational lifetime.

Fuel cell durability can be improved through mitigation strategies developed from an understanding of the various factors that contribute to their reduced performance and produce degradation under the operating conditions. Given

* *Corresponding author.*
E-mail address: ekjeang@sfu.ca (E. Kjeang).
http://dx.doi.org/10.1016/j.ijhydene.2017.06.151

the complex interplay of multiple physical phenomena that are simultaneously active in a running fuel cell, the origin of degradation factors can be multi-faceted. Additionally, the types of degradation mechanisms can differ in various components of the operating fuel cell assembly, *viz.* Membrane, catalyst layers (CLs), gas diffusion layers (GDLs), and bipolar plates [2].

In a polymer electrolyte membrane (PEM) fuel cell, one of the critical functions of the membrane is to physically separate the fuel and oxidant, thereby enabling the electrochemical reaction and consequential electrical power generation. During fuel cell operation, transitions between low and high power demands produce temperature and humidity (collectively known as 'hygrothermal') variations in the membrane. Because the membrane is mechanically constrained within the fuel cell, its dynamic water sorption characteristics during hygrothermal variations translate into cyclic mechanical stresses and strains, which can cause severe fatigue that may initiate micro-cracks at locations with high stress concentration [3–6]. Commonly used perfluorosulfonic acid (PFSA) ionomer membranes (e.g., Nafion) exhibit an elastic-viscoplastic behaviour due to which their mechanical properties, such as Young's modulus, yield strength, and post-yield strain hardening, are a function of the rate of applied loading [7]. As the cyclic stresses generated within the membrane are a result of hygrothermal cycling, the mechanical properties accordingly vary with the rate of this cycling. Within the typical operating range of 23–70 °C temperature and 50–90% RH, Goulet et al. [8] reported a significant variation in the mechanical properties of both pure membranes and catalyst coated membranes (CCMs). They also showed, in a separate study, that the pure membranes generate twice as much longitudinal peak and residual stress during dehydration than the CCMs [9]. Nevertheless, cracks in the catalyst layers still influence membrane crack development by acting as preferential crack initiation sites due to stress concentration effects [10]. Under continued cycling of mechanical stresses, micro-cracks can propagate through the membrane, opening up a pathway for direct chemical reaction between the fuel and oxidant, thereby compromising the very functionality of the membrane and diminishing its structural integrity [11]. The reactant leakage is also a potential safety hazard due to the potentially combustive gas mixture formed, and is therefore considered a lifetime limiting failure mode.

Researchers have attempted to understand the effect of operating conditions on the PEM fuel cell membrane durability and some of these investigations have led to the development of suitable degradation mitigation strategies. The mechanical stability of the membrane was found to be significantly affected by cyclic changes in the environmental conditions, and in particular, by cyclic changes of relative humidity (RH) [12]. Dimensional change (or strain) induced by water uptake was found to be a major cause for the mechanical degradation and failure of the membranes [5]. Lai et al. [13] and Kusoglu et al. [14] showed that the lifetime of a membrane decreases with increasing oscillations of its water content during RH cycling. According to Aindow et al. [6], when membranes are subjected to cyclic mechanical stresses at 60 °C and 90% RH, their lifetime decreases exponentially with the applied stress levels. Khorasany et al. [15] conducted a comprehensive *ex situ* experimental investigation of membrane fatigue lifetime by subjecting dogbone-shaped samples to cyclic mechanical loading and found the time taken for failure initiation to be a strong function of applied stress, temperature, and relative humidity. Moreover, temperature was found to have a relatively greater effect than humidity. In a recent work, Sadeghi Alavijeh et al. [16] also reported the accumulation of significant creep damage in the CCM material during cyclic stress conditions, which could have an added detrimental effect on the fuel cell durability.

Chemical membrane degradation is also important, and both chemical and mechanical degradation are known to occur concurrently during fuel cell operation through a complex, coupled mechanism [17]. Sadeghi Alavijeh et al. reported decay in mechanical properties due to the action of combined chemical and mechanical stressors [18]. Wong et al. [19] developed a chemical membrane degradation model to determine the linkages between the reaction-transport phenomena in the membrane electrode assembly, *in situ* operating conditions, and the temporal membrane degradation process. In fuel cell membranes, traces of Fe^{II} ions can be present due to contamination during fabrication and/or operational stages [20] and are found to have a severe deleterious impact on the rate of chemical degradation in the membrane [21]. Wong et al. [22] suggested that sustained intermediate cell voltage operation could efficiently mitigate chemical membrane degradation due to reduced Fe^{II} concentration. Lim et al. [17] applied an advanced accelerated stress test (AST) protocol to study the simultaneous effect of chemical and mechanical degradation mechanisms. They found pinhole and crack formations leading to hydrogen leakage as the primary cause of failure in the membranes [17] and identified the addition of CeO_2 to the fuel cell electrodes as a mitigation strategy for durability enhancement [23]. The CeO_2 applied on the electrodes is believed to be dissolved into Ce ions which migrate into the membrane and reduce the rate of chemical degradation through hydroxyl radical scavenging [23]. Macauley et al. [24] designed and validated an accelerated membrane durability test (AMDT) protocol customized for heavy duty fuel cells used in transit bus applications and reported that the Pt band in the membrane significantly decreases the rate of membrane degradation, thereby enhancing its longevity [25].

The nature of mechanical degradation and overall durability of PEM fuel cell membranes during typical operating conditions has been well investigated. Experiments were conducted by Li et al. [26] and Patankar et al. [27] to characterize the intrinsic fracture energy G_c of polymeric membranes. G_c is a threshold value below which the crack growth is sub-critical and therefore, harmless. Moreover, G_c was found to be more sensitive to temperature than humidity [27]. Poornesh et al. [28] investigated damage propagation at interfaces and found that the fracture properties of the layer from which damage initiates has an important effect on crack propagation. The interlinkage between membrane damage and structure/properties of the adjacent CL and GDL was also demonstrated in several investigations carried out by Uchiyama et al. [29–31] from Toyota Motor Corporation. Kai et al. [32,33] from the same group studied deformation and fatigue under static and cyclic mechanical loading as well as

humidity cycling, and found that crack formation in the CL occurs immediately after yielding and with increasing tensile strain, the number of new CL cracks as well as the length and width of the existing cracks increase. Kusoglu et al. used finite element analysis to study the evolution of *in situ* stresses and plastic deformation in fuel cell membranes during humidity cycling [4,34] and further extended it to develop a numerical model based on craze initiation criteria that explained critical qualitative aspects of the membrane fatigue behaviour [14]. Khorasany et al. also developed a finite element based numerical model capable of predicting the spatial distribution of lifetime within a fatigue loaded membrane sample under both *ex situ* [35] and *in situ* [36] hygrothermal cycling conditions. Banan et al. [37–39] developed finite element models to study the individual and combined effects of mechanical vibrations and hygrothermal cycling on delamination of membrane-CL interface and crack propagation within membranes. In their simulations, frequency of vibrations was found to have a dominant effect on delamination whereas crack propagation was affected more by hygrothermal cycling. More recently, Ding et al. [40,41] utilized a plastic energy dissipation criterion to model crack growth in polymers and demonstrated its utility in capturing important fuel cell related experimental observations such as improved durability of mechanically reinforced membranes and higher susceptibility of membrane damage under the flow channels during humidity cycling. Despite this body of work, there remains a lack of sufficient literature that particularly addresses the fundamental nature of crack/damage propagation behaviour through the membranes and provides a model that is validated strictly against the empirical evidence.

Membrane durability has recently been a subject of extensive research within our group and mechanical degradation, in particular, has been investigated systematically through a range of focused experimental and/or modelling efforts. Characterization of mechanical properties [8], water sorption and expansion properties [9], pure creep behaviour [16], pure fatigue (or crack initiation) behaviour [15,42], and combined creep-fatigue behaviour [43] has been reported so far. The work presented here is designed to complement this body of knowledge with a focused investigation on the crack propagation behaviour. The objective of this work is to bridge the existing gap in the literature to specifically understand the fundamentals of mechanical fatigue-based crack propagation in automotive fuel cell membranes. It involves the development of a novel and comprehensive *ex situ* experimental investigation strategy, similar to the fatigue testing performed by Khorasany et al. [15], to gauge the effects of stress level, temperature, and humidity on the rate of crack propagation in standard ionomer membranes. The experiments are performed by subjecting a rectangular specimen with double edge cracks of known initial length to cyclic uniaxial tensile mechanical loading and measuring the increase in crack length which is then used to determine the average crack growth rate. The experimental investigations are complemented by microstructural analysis of the membrane's surface morphology around the fracture surface and crack tip to develop a better insight into the physical processes involved during crack propagation. Finally, a simulation tool is developed which integrates the experimental findings on stress, temperature, and humidity dependent crack growth behaviour with relevant analytical and computational models. The tool, based on Paris Law theory [44], is capable of predicting the fatigue-driven crack growth in the membranes when subjected to cyclic mechanical stresses and, therefore, can be potentially useful in mitigating some important factors that curtail the overall fuel cell durability in automotive applications.

Experimental investigation

Experimental materials

Commercially available Nafion NRE 211 perfluorosulfonic acid (PFSA) ionomer membrane of 25 μm thickness was used for the experimental analysis of crack propagation. To ensure consistency between the results, a single batch of material was used. Test articles were cut in rectangular shapes of 10 mm width and 20 mm length, as illustrated in Fig. 1. The variations in the dimensions were less than 1%. A custom-made die with blades made from hardened steel was used to create small, consistent cracks on both sides of the test articles (cf., Fig. 1a). The length of the crack (a) on each side was 0.7 mm, with a variation of less than 2% to ensure adequate specimen symmetry. The quality of the obtained specimens was visually confirmed with an optical microscope before testing. If any inconsistencies in the cuts were observed, the specimen was rejected and if necessary, the die was replaced with a new one.

Experimental procedure

The *ex situ* crack propagation experiments were performed using a Dynamic Mechanical Analyzer (TA Instruments Q800 DMA) with humidity accessory. Initially the specimen was loaded in the DMA and equilibrated under a small preload force (~0.001 N) at room conditions. Then, using the humidity accessory, the environmental conditions of the test were elevated to desired levels followed by renewed specimen equilibration. This test initiation procedure is necessary in order to avoid interferences of stresses generated by variations in the environmental condition during testing. The increase in specimen length during this process was monitored, and equilibrium was assumed once the dynamic change in length was less than 0.01% of the original length. During the crack propagation test, a constant mean tensile force combined with a sinusoidal cyclic force (Fig. 1b) was applied normal to the width of the specimen at the free end while the opposite end was clamped (Fig. 1a). The frequency of the cyclic loadings was selected to be 10 Hz, while the amplitude was chosen based on a minimum to maximum applied stress ratio (R) of 20%, in accordance with our previous experimental and modelling works [15,35].

It should be noted that in an operating fuel cell, mechanical fatigue stresses develop within the membrane due to its cyclic expansion and contraction caused by dynamic temperature and/or humidity fluctuations. If the compressive stress produced during constrained expansion surpasses the elastic regime, residual tensile stresses develop during contraction

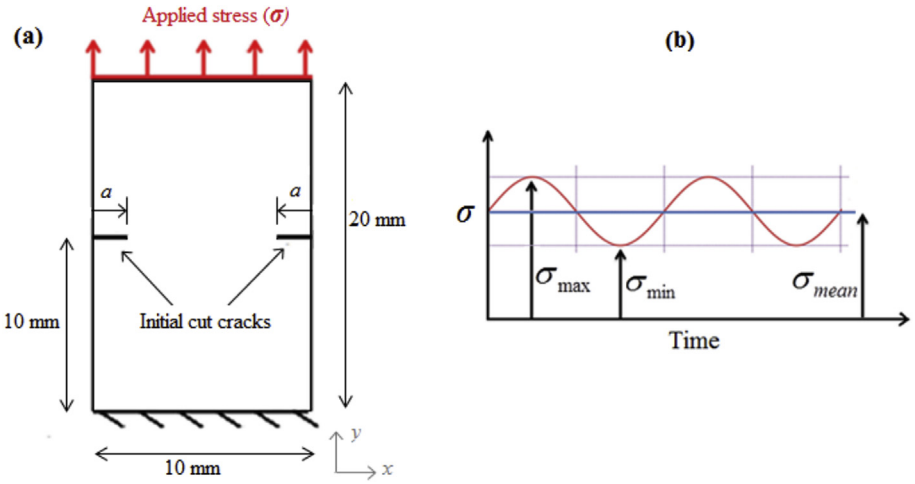

Fig. 1 – (a) Double edge crack specimen of membrane with initial cut cracks of length $a = 0.7$ mm on each side and (b) tensile fatigue stress profile applied during the *ex situ* experiments. σ_{max}, σ_{min}, and σ_{mean} represent the maximum, minimum, and mean values of the sinusoidal stress profile, respectively.

which are capable of initiating and propagating cracks within the membrane material [14]. Due to the slow response to temperature and humidity cycling, however, *ex situ* crack growth rate characterization under such conditions could be prohibitively time consuming. This work utilizes an idealized experimental approach in which dynamic *in situ* tensile stress levels (up to 9 MPa) within the membrane, which have been reported based on finite element simulations [45], are rapidly generated via applied force under typical temperature (23–70 °C) and RH (50–90%) ranges encountered in an automotive fuel cell [8]. The selected load cycle frequency is also considerably higher than for the hygrothermal stress cycles experienced by the membrane during fuel cell operation in order to accelerate the test. Therefore, the present experimental technique is expected to capture a purely fatigue-induced crack propagation process, and viscoelastic effects such as creep deformation are thus beyond the scope of this work. For each environmental condition, four different levels of stress amplitude were used in order to obtain a reliable crack propagation of approximately 30–40% of the original crack length within a reasonable experimental time. The experiments were repeated at least three times at each condition. Goulet et al. [8] reported that the yield strength (σ_Y) of the membrane decreases with both increasing temperature and humidity; therefore, the σ_{max} values at each environmental condition were chosen to lie within the measured yield strength for 0.1 min^{-1} strain rate [8] in order to realize a predominantly elastic deformation within the bulk of the test specimen. The area used to calculate these applied stress levels was determined using the specimen width measured at the cross-section bearing the initial crack, i.e., $(10 - 2a)$ mm as per Fig. 1a, to further ensure that the bulk stress levels remained within the elastic regime. The individual length of the left and right side cracks was measured before and after each experiment using an optical microscope. An average value of crack growth rate was then deduced for each experiment using the incremental crack length and experiment duration.

The change in membrane surface morphology and structural features during crack propagation was investigated for one experimental sample using a ZEISS Xradia VersaXRM-520® X-ray computed tomography (XCT) system. After the fracture experiments, the membrane specimen was fastened to a rigid plastic support using an adhesive tape to prevent sample movement during tomography acquisition. The plastic-supported specimen was placed on the rotation stage of the XCT system using a clip-type sample holder. The X-ray source was operated at 7 W power and 80 kV voltage; and a 20× detector was used to capture the photons. A total of 1601 2D images, each with an exposure time of 50 s, were captured for a complete 360° rotation of the sample. Zeiss' proprietary XMR Reconstructor® software was then used to reconstruct the set of 2D images acquired during tomography into a viewable 3D digital image.

Experimental results and discussion

Tensile fatigue-based crack propagation experiments were conducted under a comprehensive range of applied cyclic mechanical loading, temperature, and relative humidity conditions. The specimen elongation monitored during the experiments was determined to be less than 2–3% of the initial length, indicating that the applied tensile stress profile was kept in the elastic regime for the bulk specimen material, which is expected to be realistic for fuel cell conditions and provide relevant results using the fatigue characterization approach adopted here. However, the local stress at the crack tip is expected to be higher, and hence drive the crack growth. The average crack propagation rates were calculated for both cracks on the left and right sides of the specimen and are plotted in Fig. 2 against the bulk stress amplitude $\Delta\sigma$ $(\sigma_{max} - \sigma_{min})$ applied during sinusoidal mechanical loading. The crack propagation rates in this figure are shown on a logarithmic scale for experiments conducted under four different sets of environmental conditions and each data point represents an average from 3 to 4 tests. Crack

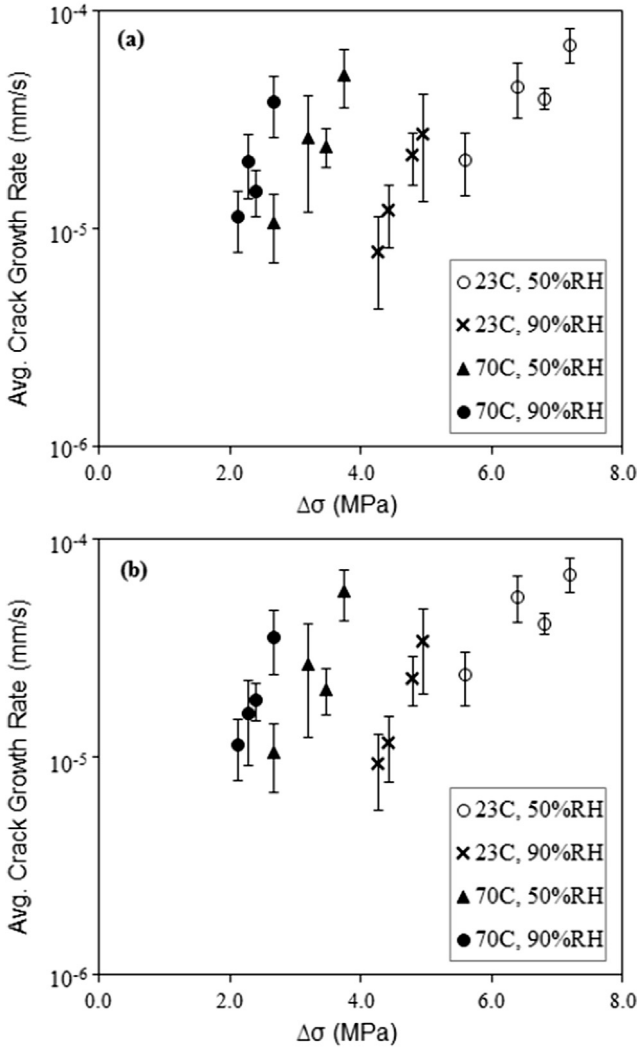

Fig. 2 – Experimentally measured crack growth rate as a function of applied stress amplitude ($\Delta\sigma$) and environmental conditions for the (a) left and (b) right side cracks.

propagation under fatigue loading, such as the present case, is driven by confined plasticity around the crack tip due to stress concentration effects [46]. Microscale differences between the left and right crack geometries could lead to differences in the concentrated stress values and therefore, deviations in crack propagation rates of the two sides may be encountered. In the present case, small deviations between the left and right cracks were observed; however, the general trends between the two were consistent. A visual inspection of the curves indicates that for a given environmental condition, the rate of crack growth with respect to the applied stress amplitude was nearly identical for the left and right side cracks. The typical crack propagation rates were on the order of 10^{-5} to 10^{-4} mm s^{-1}, which is equivalent to 30–300 μm per hour of experimental time or 1–10 μm per 1000 fatigue cycles.

The crack growth rate was highly sensitive to the applied stress level. For instance, a 10–30% increase in $\Delta\sigma$ (depending on the RH and T levels) resulted in a corresponding order of magnitude increase in the crack growth rate. Due to the presence/development of catalyst layer cracks and other spatial non-uniformities in an operating fuel cell, stress concentration regions are expected to exist within the membrane [47]. Moreover, *in situ* simulations of fuel cells have predicted higher in-plane tensile stress levels under the flow field channels than under the lands [45]. The high sensitivity of crack growth to applied stress observed in this work indicates that cracks would propagate faster in the aforementioned high stress regions and therefore, stress non-uniformity within the membrane is identified as a critical factor affecting its overall fatigue durability.

As the temperature and relative humidity were increased during the experiments, the stress amplitude applied to the specimen had to be reduced; otherwise the specimen was found to rupture instantly. This requirement of adjustment in the applied stress essentially indicates that the membrane material becomes less resistant to crack growth at higher temperature and humidity conditions. To achieve a given growth rate, the required reduction in $\Delta\sigma$ from room conditions (23 °C, 50% RH) was about 10–15% for humidity increase from 50 to 90% RH and 35–40% for temperature increase from 23 to 70 °C. These observations indicate that the temperature has a stronger effect on fracture propagation than humidity. In a previous work, Patankar et al. [27] reported that the intrinsic fracture energy G_c, which is the threshold for crack initiation, is more sensitive to temperature than humidity. The present observations reveal that the same trend in sensitivities also continues after the crack propagation has begun.

The sensitivity of the crack growth rate to $\Delta\sigma$ is also found to increase at elevated levels of environmental conditions as seen from the increasing slope values of the plots in Fig. 2. For example, the crack growth is about twice as sensitive to $\Delta\sigma$ at fuel cell conditions (70 °C, 90% RH) than at the room conditions. This sensitivity change is attributed to the fact that at elevated levels of environmental conditions, the membrane exhibits lower pre and post yield moduli [8]. Hence, a small change in the applied stress level can create a significant change in the release rate of fracture energy stored in the specimen due to the distributed strain around the crack tip. Furthermore, the temperature is found to increase the crack growth rate sensitivity to $\Delta\sigma$ more substantially than the relative humidity within the tested range. This is again due to the greater effect of temperature on the moduli of the material and associated release rate of strain energy. Hence, in the context of fuel cell operation at elevated levels of environmental conditions, a small change in stress magnitude may create a dramatic change in strain. A reduction in $\Delta\sigma$ at such elevated conditions can therefore significantly reduce the crack propagation rate by means of a lower release rate of strain energy due to the lower strain around the crack tip. The results obtained here are in overall agreement with the fatigue results previously reported by our group [15], where the severity of mechanical fatigue was found to increase considerably with temperature.

Fig. 3 shows a representative 3D virtual image of the propagated fracture region of the membrane specimen after being subjected to a stress amplitude $\Delta\sigma$ of 5.0 MPa at 23 °C and 90% RH, revealing the geometry of the fracture surface and crack tip with a voxel size and spatial resolution of approximately 1 μm. The original thickness of the specimen

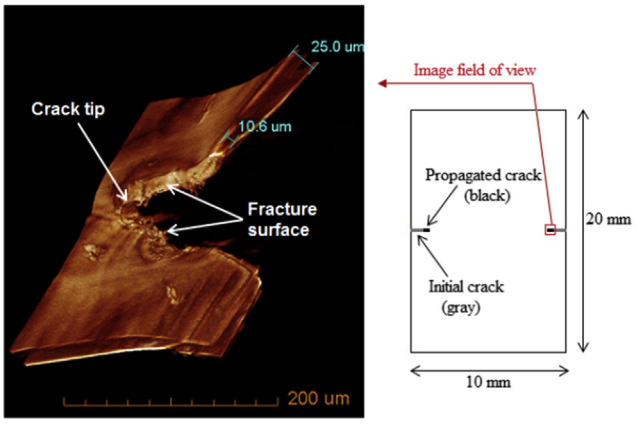

Fig. 3 – 3D virtually reconstructed image of the fracture region of a membrane specimen subjected to fatigue-driven crack propagation under stress amplitude of 5.0 MPa at 23 °C and 90% RH. The scaled illustration on the right indicates the field of view of the image within the overall specimen geometry.

was 25.0 ± 1.1 μm, as depicted in the measurement taken sufficiently far away from the fracture surface. In regions close to the fracture surface, however, the thickness was reduced to 10.6 μm, indicating a substantial plastic (permanent) deformation around the crack surface. Moreover, the continuous undulation of the crack surface morphology appears to be the fatigue striations which are typical of ductile fatigue fracture driven by localized plastic deformation [46]. On the other hand, the absence of such plastic deformation in regions away from the fracture surface indicates that the bulk of the specimen experienced stresses that were below the critical yield strength (σ_Y). It should be noted that the field of view of the virtual image in Fig. 3 is extremely small compared to the overall dimensions of the tested sample, as evident from the scaled illustration, which confirms the high degree of localization of the plastic deformation during fatigue cycling. Therefore, it is the concentrated stress around the propagating crack tip that produces confined plasticity around it while the rest of the specimen deforms elastically. This is a typical case of the fatigue-driven crack propagation phenomenon that can be modelled using the empirical Paris Law theory [46] and justifies the modelling approach adopted in this work which is discussed later.

Fracture model development

The *ex situ* experimental results described in the previous sections provide valuable insights into the effect of operating conditions on the crack propagation behaviour inside polymeric membranes. Parameters derived from the experimental results were further utilized in conjunction with analytical fracture mechanics fundamentals to develop a semi-empirical framework for membrane fracture growth simulation. The peculiarity of elastic-viscoplastic mechanical behaviour of membranes introduces an added layer of complexity while trying to simulate crack propagation. To ensure that the mechanical behaviour of membranes is accurately captured, a temperature and humidity dependent elastic-viscoplastic constitutive model was first developed in COMSOL Multiphysics® and all subsequent crack propagation simulations were based upon this model. The fracture model development was, therefore, carried out in two steps; each dedicated individually to the development of: (1) an elastic-viscoplastic constitutive model, and (2) a semi-analytical crack propagation model. Their details and integration process are described in the following sub-sections.

Elastic-viscoplastic constitutive model

Theory

The structure of polymeric membranes is in the form of a molecular network with interconnected molecular chains [45]. Any deformation (strain) in the membrane is resisted (stress) by two types of simultaneously active mechanisms: (A) *Intermolecular*, and (B) *Network*. The *intermolecular mechanism*, represented by a linear elastic spring in series with a viscoplastic dashpot, is the main stress contributor at relatively low strains. The contribution to the overall stress from the *network mechanism*, represented by a non-linear elastic spring, becomes significant only at high strain levels. In the remainder of this section, subscripts *A* and *B* are used to identify variables that are specific to the *intermolecular* and *network mechanisms*, respectively, while the non-subscripted variables apply to the overall membrane material. Because the two mechanisms act in parallel, the overall Cauchy stress ($\boldsymbol{\sigma}$) developed in the membrane is a sum of stress contributions from both mechanisms, i.e.

$$\boldsymbol{\sigma} = \boldsymbol{\sigma}_A + \boldsymbol{\sigma}_B \tag{1}$$

where $\boldsymbol{\sigma}_A$ and $\boldsymbol{\sigma}_B$ are the individual stress contributions from the *intermolecular* and *network mechanisms*, respectively. The deformation gradients (denoted by **F**), however, are the same in both mechanisms, i.e.

$$\boldsymbol{F}_A = \boldsymbol{F}_B \tag{2}$$

When deformations are large, the concept of multiplicative decomposition of the deformation gradient into elastic and plastic parts is generally employed for polymeric materials [48]. In the *intermolecular mechanism*, this involves the breakdown of overall deformation gradient ($\boldsymbol{F}_A$) into elastic and plastic components according to

$$\boldsymbol{F}_A = \boldsymbol{F}_A^e \boldsymbol{F}_A^p \tag{3}$$

where $\boldsymbol{F}_A^e$ and $\boldsymbol{F}_A^p$ are the elastic and plastic portions of the deformation gradient from the *intermolecular mechanism*, respectively.

The stress in the *intermolecular mechanism* ($\boldsymbol{\sigma}_A$) is produced due to the elastic component of deformation only and can be calculated as

$$\boldsymbol{\sigma}_A = 2\mu_A \boldsymbol{\varepsilon}_A^{e\prime} + \kappa_A tr(\boldsymbol{\varepsilon}_A^e) I \tag{4}$$

where μ_A and κ_A are the shear and bulk moduli for the *intermolecular mechanism*, respectively; $\boldsymbol{\varepsilon}_A^e = \frac{1}{2}(\boldsymbol{F}_A^{eT}\boldsymbol{F}_A^e - \boldsymbol{I})$ is the strain tensor for the elastic component of the *intermolecular mechanism* where *I* is the 2nd order identity tensor and superscript *T*

represents the matrix transpose; function $tr()$ calculates the trace of the matrix argument; and $\varepsilon_A^{e\prime}$ refers to the deviatoric part of the strain tensor $\boldsymbol{\varepsilon}_A^e$. As a corollary, Eq. (4) enables evaluation of the elastic deformation gradient ($\mathbf{F}_A^e$) from the stress levels in the *intermolecular mechanism*.

The plastic flow in the *intermolecular mechanism* is initiated and propagated by shear stresses [49] that are expressed using the deviatoric component (identified by superscript ′) of the stress tensor given by

$$\boldsymbol{\sigma}'_A = \boldsymbol{\sigma}_A - \frac{1}{3}(\sigma_{A\_11} + \sigma_{A\_22} + \sigma_{A\_33})\boldsymbol{I} \tag{5}$$

where σ_{A_11}, σ_{A_22}, and σ_{A_33} are the stress components in the three principal directions. The Frobenius norm of the deviatoric stress tensor ($\boldsymbol{\sigma}'_A$) can be calculated as

$$\tau_A = \left(tr\left[(\boldsymbol{\sigma}'_A)^T \boldsymbol{\sigma}'_A\right]\right)^{1/2} \tag{6}$$

and is used to determine the direction of the driving stress for plastic deformation given by

$$N_A = \frac{\boldsymbol{\sigma}'_A}{\tau_A} \tag{7}$$

The plastic velocity gradient for the *intermolecular mechanism* ($\boldsymbol{L}_A^p$) can be obtained from its corresponding deformation gradient ($\mathbf{F}_A^p$) using the following relationship of continuum mechanics

$$\boldsymbol{L}_A^p = \dot{\mathbf{F}}_A^p (\mathbf{F}_A^p)^{-1} \tag{8}$$

where the dot indicates time derivative. Additionally, the plastic velocity gradient can be expressed as a summation of contributions from the rates of plastic stretching ($\boldsymbol{D}_A^p$) and plastic spin ($\mathbf{W}_A^p$), i.e.

$$\boldsymbol{L}_A^p = \boldsymbol{D}_A^p + \mathbf{W}_A^p \tag{9}$$

where $\boldsymbol{D}_A^p$ and $\mathbf{W}_A^p$ represent the symmetric and skew-symmetric parts of matrix $\boldsymbol{L}_A^p$ [48]. Assuming the plastic flow to be irrotational ($\mathbf{W}_A^p = 0$) and using Eqs. (8) and (9), we can write

$$\boldsymbol{D}_A^p = \dot{\mathbf{F}}_A^p (\mathbf{F}_A^p)^{-1} \tag{10}$$

In terms of the driving stresses described in Eq. (7), the rate of plastic stretching is also given by the following relationship

$$\boldsymbol{D}_A^p = \dot{\gamma}_A^p \mathbf{N}_A = \dot{\gamma}_A^p \frac{\boldsymbol{\sigma}'_A}{\tau_A} \tag{11}$$

where $\dot{\gamma}_A^p$ is a measure of the plastic flow rate of the material for the *intermolecular mechanism*. $\dot{\gamma}_A^p$ is obtained by factoring in the effect of plastic deformation, stress, and temperature on the inherent rate-dependent yield ($\dot{\gamma}_0$) using the following reptation-inspired equation that was originally developed for elastomers in the work of Bergstrom and Boyce [50] and later utilized by Yoon et al. [48] to capture the rate dependent response of Nafion material

$$\dot{\gamma}_A^p = \dot{\gamma}_0 [\lambda^p - 1]^c \cdot \left(\frac{\tau_A}{\tau_{base} + \beta p^e}\right)^M \cdot \left(\frac{T}{T_{base}}\right)^n \tag{12}$$

where $\lambda^p = \sqrt{tr(\boldsymbol{B}_A^p)/3}$ is an effective plastic chain stretch and $\boldsymbol{B}_A^p = \mathbf{F}_A^p (\mathbf{F}_A^p)^T$ is the left Cauchy-Green plastic deformation tensor for the *intermolecular mechanism*. The term $[\lambda^p - 1]^c$ captures a stretch dependence of the effective viscosity with material constant $c \in [-1,0]$ and is a key component to capturing the rate-dependent behaviour [50]. Additionally, $\left(\frac{\tau_A}{\tau_{base} + \beta p^e}\right)^M$ and $\left(\frac{T}{T_{base}}\right)^n$ are thermally motivated phenomenological terms affecting the plastic flow rate where $p^e = -\frac{1}{3}(\sigma_{A\_11} + \sigma_{A\_22} + \sigma_{A\_33})$ is the hydrostatic pressure in the *intermolecular mechanism*, T is the temperature in °C, and τ_{base} (in units of shear modulus μ_A), β, M, T_{base} (in °C), and n are phenomenological material parameters with values for Nafion reported in Ref. [48] and presented in Table 1. Eqs. 10 and 11 can be combined to express the plastic deformation gradient ($\mathbf{F}_A^p$) in the form of a differential equation in time as

$$\dot{\mathbf{F}}_A^p = \left(\dot{\gamma}_A^p \frac{\boldsymbol{\sigma}'_A}{\tau_A}\right) \mathbf{F}_A^p \tag{13}$$

This differential equation can be solved for $\mathbf{F}_A^p$ which consequently enables the evaluation of the *intermolecular mechanism's* overall deformation gradient ($\mathbf{F}_A$) using Eq. (3). It should be noted that $\dot{\gamma}_A^p$ is a highly non-linear function of plastic deformation, stresses, and temperature and therefore introduces a substantial computational demand while solving Eq. (13), particularly under dynamic conditions.

The contribution of the *network mechanism's* resistance to the total stress can be calculated as

$$\sigma_B = \frac{1}{J_B} \mu_B \mathbf{B}'_A \tag{14}$$

where $\mathbf{B}_B = \mathbf{F}_B \mathbf{F}_B^T$ is the left Cauchy-Green tensor of the *network mechanism's* deformation gradients, μ_B is its shear modulus, and $J_B = \det(\mathbf{F}_B)$. The prime symbol ($\prime$) represents the deviatoric part of the tensor.

It should be noted that several material parameters ($\mu_A, \dot{\gamma}_0, \tau_{base}, \mu_B$) are a function of temperature, humidity, and/or loading rate. The exact form of this functional relationship was determined using the experimental results reported by Goulet et al. [8] and is mathematically expressed using the sensitivity factors given in Table 1.

Model description

Based on the theory presented in the previous section, a finite element model was developed in COMSOL Multiphysics® 4.3 to simulate the elastic-viscoplastic response of fuel cell membranes at various temperature, relative humidity, and loading rate conditions. It must be emphasized that the capability of COMSOL Multiphysics® to simulate the elastic-viscoplastic phenomenon is very limited. The present model, therefore, makes use of the linear elastic sub-model representing the elastic part of the *intermolecular mechanism* as the foundation. This sub-model evaluates the elastic deformation gradients ($\mathbf{F}_A^e$) and stress ($\boldsymbol{\sigma}_A$) only. The Equation Based Modelling® feature of COMSOL Multiphysics® was utilized to solve Eq. (13) and evaluate the plastic deformation gradients ($\mathbf{F}_A^p$). The stress in the *network mechanism* ($\boldsymbol{\sigma}_B$) was evaluated using both $\mathbf{F}_A^e$ and $\mathbf{F}_A^p$ which are related to $\mathbf{F}_B$ according to Eqs. (2) and (3).

The model presented here was developed specifically for the Nafion NRE211 membrane material but can be generally

Table 1 – Material properties of Nafion NRE211 at reference conditions, i.e., T_{ref} = 23 °C, RH_{ref} = 50%, and SR_{ref} = 0.0001 s^{-1} [45,48]; and their sensitivity to temperature (T), relative humidity (RH), and strain rate (SR).

Material parameter	Value at reference conditions	Sensitivity factor
μ_A	97 MPa	$\left[1-0.45^{\frac{(RH-RH_{ref})}{(90-RH_{ref})}}\right] \times \left[1-0.50^{\frac{(T-T_{ref})}{(70-T_{ref})}}\right]$
κ_A	210 MPa	1
$\dot{\gamma}_0$	1 s-1	$\left[1+0.611^{\frac{(SR-SR_{ref})}{SR_{ref}}}\right] \times \left[1-0.033^{\frac{(SR-SR_{ref})}{SR_{ref}}\cdot\frac{(T-T_{ref})}{(70-T_{ref})}}\right] \times \left[1-0.044^{\frac{(SR-SR_{ref})}{SR_{ref}}\cdot\frac{(T-T_{ref})}{(70-T_{ref})}\cdot\frac{(RH-RH_{ref})}{(90-RH_{ref})}}\right]$
c	−0.5	1
M	1.52	1
τ_{base}	1.42 × μ_A	$e^{[2.9(T-T_{ref})/(70-T_{ref})]}$
β	0.6	1
n	4.5	1
T_{base}	100 °C	1
μ_B	2.67 MPa	$\left[1+0.38\times\frac{(RH-RH_{ref})}{(90-RH_{ref})}\right] \times \left[1-0.28\times\frac{(T-T_{ref})}{(70-T_{ref})}\right]$

utilized for any polymer exhibiting elastic-viscoplastic behaviour by implementation of appropriate material property values. These values for Nafion NRE211 are listed in Table 1. Given the dependency of certain material properties on temperature, humidity, and loading rate, the values are specified at reference temperature T_{ref} = 23 °C, relative humidity RH_{ref} = 50%, and strain rate SR_{ref} = 0.0001 s^{-1} conditions. The geometry and loading conditions were selected in accordance with the *ex situ* tensile experiments performed by Goulet et al. [8], as illustrated schematically in Fig. 4a. As the specimen thickness is two orders of magnitude less than the length and width, the *plane stress* simplification was adopted to facilitate a 2-D analysis in the *x*-*y* plane. The membrane was fixed at one end and stretched along its length with a constant uniaxial strain rate (SR) at the other end to produce a tensile strain along its longitudinal direction. The temperature (T) and relative humidity (RH) were kept constant during the entire simulation so that there was no hygrothermal expansion/contraction in the membrane during the stretching process and hence T and RH only influenced the material property values given in Table 1. Two different conditions of T (23 °C and 70 °C), RH (50% and 90%), and SR (0.0001 s^{-1} and 0.001 s^{-1}) were considered in this work, and simulations were performed for all combinations of these parameters.

A 2-D 3-node free triangular element was used to mesh the membrane geometry into 42 elements. The built-in Time Discrete® solver of COMSOL Multiphysics® was used to generate a spatial solution for the displacement vector $\{\boldsymbol{u}\}$ and plastic deformation tensor $[\boldsymbol{F}_A^p]$ at time intervals of Δt = 100 s using initial displacement vector $\{\boldsymbol{u}_0\} = \{0\}$ (zero vector), initial velocity vector $\{\dot{\boldsymbol{u}}_0\} = \{0\}$, $[\boldsymbol{F}_A^p] = [I]$ (identity matrix), and $[\dot{\boldsymbol{F}}_A^p] = [0]$ (zero matrix). Mesh independence and convergence were ensured in all simulations. The solutions were post-processed to obtain stress versus strain curves at point A, located at the right edge of the specimen (cf., Fig. 4a).

Model validation

Fig. 4b shows a comparison of membrane stress-strain results obtained from the simulations of the *Elastic-Viscoplastic Constitutive Model* and those reported by Goulet et al. [8] for *ex situ* experiments. This set of results is for a constant SR of 0.0001 s^{-1} and four different combinations of T (23 °C and 70 °C) and RH (50% and 90%) conditions. The data presented here depict the true stress and true strain values measured/computed at point A.

The simulation results show a good agreement with the experimental data which validates the capability of the developed model to simulate the elastic-viscoplastic behaviour of the membrane at the reported conditions. It is worth noting that the typical characteristics of the membrane response, *viz.* initial linear elasticity, gradual yielding, and plastic strain with isotropic-hardening, were accurately captured in the simulated results. The decrease in elastic modulus and yield strength with increasing temperature and humidity, as seen in the simulated results, is consistent with the common knowledge about polymeric membranes [8]. In the post-yield region, there is a discernible decrease in the isotropic-hardening of plastic strain (i.e., plastic region slope) when the temperature is increased from 23 °C to 70 °C;

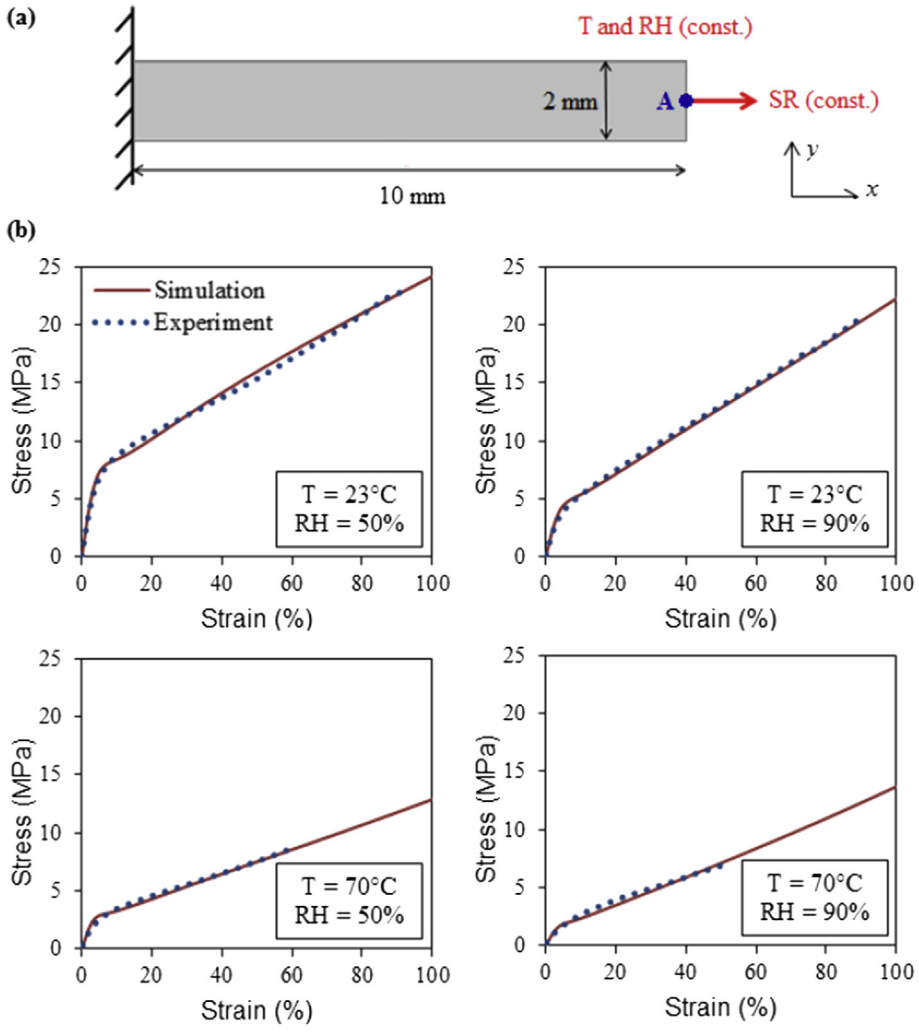

Fig. 4 – (a) Geometry and loading for a membrane specimen during the *ex situ* tensile test simulations; and (b) comparison of *ex situ* simulation and experimental [8] results for the specimen subjected to constant uniaxial strain rate of 0.0001 s^{-1} at different temperature (T) and relative humidity (RH) conditions.

however, this variation is effectively negligible when the relative humidity is increased from 50% to 90%.

The effect of loading rate on the elastic-viscoplastic behaviour of the membrane is presented in Fig. 5 for two different conditions: *Fast* with SR = 0.001 s^{-1} and *Slow* with SR = 0.0001 s^{-1}. The increase in elastic modulus and yield strength at faster loading rates (as reported in the experiments [8]) was captured accurately by the simulation results obtained from the developed model. The simulated post-yield behaviour, which is usually unaffected by the loading rate, also showed an acceptable agreement with experiments for up to 50% strain levels. For the sake of brevity, the results presented here are only for T = 23 °C and RH = 50% but similar agreement was observed at all conditions considered during this work.

The comparisons of simulated and experimental results presented in this section demonstrate the capability of the developed model to accurately predict, both qualitatively and quantitatively, the elastic-viscoplastic mechanical behaviour of the membrane. The simulation accuracy was found to be consistent for a range of temperature, humidity, and loading

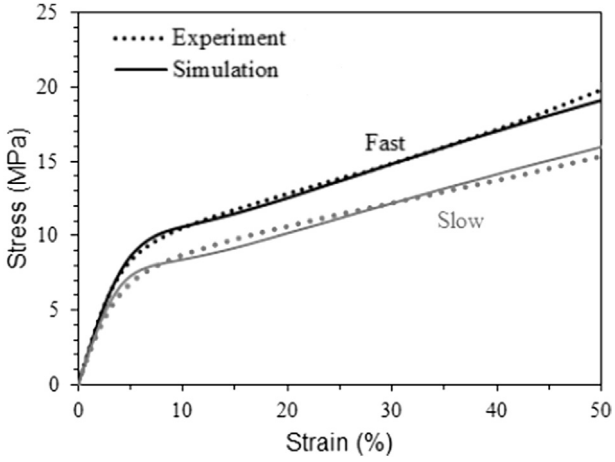

Fig. 5 – *Ex situ* simulation and experimental [8] response of the membrane at T = 23 °C and RH = 50% for fast (SR = 0.001 s^{-1}) and slow (SR = 0.0001 s^{-1}) strain rates.

rate conditions that are typically found in PEM fuel cell membranes [45]. Based on this positive validation result, the *Elastic-Viscoplastic Constitutive Model* was further applied to evaluate stress and strain dependant parameters for solving a crack propagation problem presented in the subsequent section.

Semi-analytical crack propagation model

Theory

The classical theories of elasticity and viscoplasticity assume the material to be free from any flaws or defects; however in practical situations, flaws in the form of cracks may originate in the material during manufacturing and/or due to operational stressors. When subjected to external loading, the presence of these cracks introduces a drastic change in stress distribution within the material [51]. The stress magnitudes are found to be highly concentrated around the crack tips. In elastic-viscoplastic materials, such as fuel cell membranes, stress concentrations can cause the stress levels around crack tips to exceed the yield strength values even when the bulk of the material is within the elastic regime. This results in the development of a confined plastic zone around the crack tip [46]. When the external loading is cyclic in nature, the crack face tends to repeatedly open and close and in doing so, produces a finite plastic deformation during every cycle. This plastic deformation is accompanied by an increase in the crack surface area. With every passing cycle, there is a cumulative increase in the crack surface area that translates into crack propagation through the material under cyclic loading conditions.

Based on the relative orientation of crack geometry to the applied loading direction, a crack can propagate thorough the material via combination of three mechanisms or modes: (I) opening, (II) in-plane shearing, and (III) out-of-plane shearing [37]. From the experimental results presented in Sec. Experimental results and discussion, it is clear that the plastic deformation during crack propagation is extremely confined around the crack tip while the bulk specimen experiences mechanical loading in the elastic regime. This condition is commonly referred to as small-scale yielding and theories of linear elastic fracture mechanics are applicable to such problems whereby the propensity of a crack to propagate can be quantitatively determined by evaluating stress intensity factors (K_I, K_{II}, and K_{III} for each mode) which characterize the influence of load or deformation on the magnitude of the crack tip stress and strain fields [51]. Fig. 1a shows a double edge crack specimen with cracks of length a on each side and is subjected to bulk tensile stress σ applied in vertical direction on the top edge. Such loading condition is a single mode case with only mode I responsible for crack propagation and for which the applicable stress intensity factor (K_I) around the crack tip can be calculated as

$$K_I = \sigma \cdot \sqrt{\pi a} \cdot C_c \tag{15}$$

where C_c is the configuration correction factor whose value depends upon the specimen geometry and nature of loading [52]. Typically, C_c is a non-linearly decreasing function of the crack length. When the bulk tensile stresses in Fig. 1a are cycled, the variation in stress intensity factor per cycle (ΔK_I) can accordingly be calculated as

$$\Delta K_I = \Delta\sigma \cdot \sqrt{\pi a} \cdot C_c \tag{16}$$

where $\Delta\sigma = \sigma_{max} - \sigma_{min}$ is the variation in tensile stress levels during each cycle. It is assumed here that both a and C_c remain effectively constant during a cycle, i.e., any variation in their values has a negligible contribution to ΔK_I. When σ_{max} is lower than the yield strength, the crack propagation is said to occur under fatigue loading conditions.

Paris law [44] is used to describe the crack propagation phenomenon under fatigue loading which is believed to be an important mechanical degradation mechanism in fuel cell membranes due to the development of dynamic stress patterns during automotive operation [15]. According to Paris law, the rate of crack propagation is related to ΔK_I as follows

$$\frac{da}{dN} = C(\Delta K_I)^m \tag{17}$$

where N is the number of fatigue loading cycles and C and m are material parameters which are experimentally determined from the Paris law curves plotted as $\frac{da}{dN}$ versus ΔK_I. The values of C and m are related to resistance offered by the material to fatigue-driven crack growth and are also temperature and humidity dependent [38].

The J-integral is a widely accepted fracture mechanics parameter for both linear and non-linear material responses. It is related to the energy release associated with crack growth and is a measure of the intensity of deformation at a notch or crack tip, especially for non-linear materials [51]. Although predominantly elastic deformations were maintained within the bulk of the test specimen for the experiments presented in Sec. Experimental investigation, the 25 μm thickness of the Nafion NRE 211 membrane specimen can be comparable to the size of the plastic zone that develops during the fatigue crack growth [14]. For such thin geometries, it may be necessary to utilize the J-integral for accurately capturing the elastic-plastic deformation effects around the crack tip. For a 2-D geometry, such as the one shown in Fig. 6a, the J-integral is evaluated as a line integral along a counter-clockwise contour Γ beginning on the bottom crack surface and ending on the top crack surface using the following relationship

$$J = \int_{\Gamma} \left(W dy - \mathbf{T}_i \frac{\partial \mathbf{u}_i}{\partial x} \, ds \right); \quad i = x, y \tag{18}$$

where W is the strain energy density, $\mathbf{T}$ is the traction vector, $\mathbf{u}$ is the displacement vector, and ds is an infinitesimal path length along the contour Γ, with x and y as the directions parallel and normal to the crack growth, respectively. The strain energy density is given by

$$W = \frac{1}{2}\left(\sigma_{xx} \cdot \varepsilon_{xx} + \sigma_{yy} \cdot \varepsilon_{yy} + \sigma_{xy} \cdot 2\varepsilon_{xy}\right) \tag{19}$$

where σ_{ij} and ε_{ij} are the components of the stress and strain tensors, respectively. The traction vector is defined as

$$\mathbf{T} = \begin{Bmatrix} \sigma_{xx} \cdot n_x + \sigma_{xy} \cdot n_y \\ \sigma_{yy} \cdot n_y + \sigma_{xy} \cdot n_x \end{Bmatrix} \tag{20}$$

where $\mathbf{n}$ is the normal vector to the contour Γ. If the crack

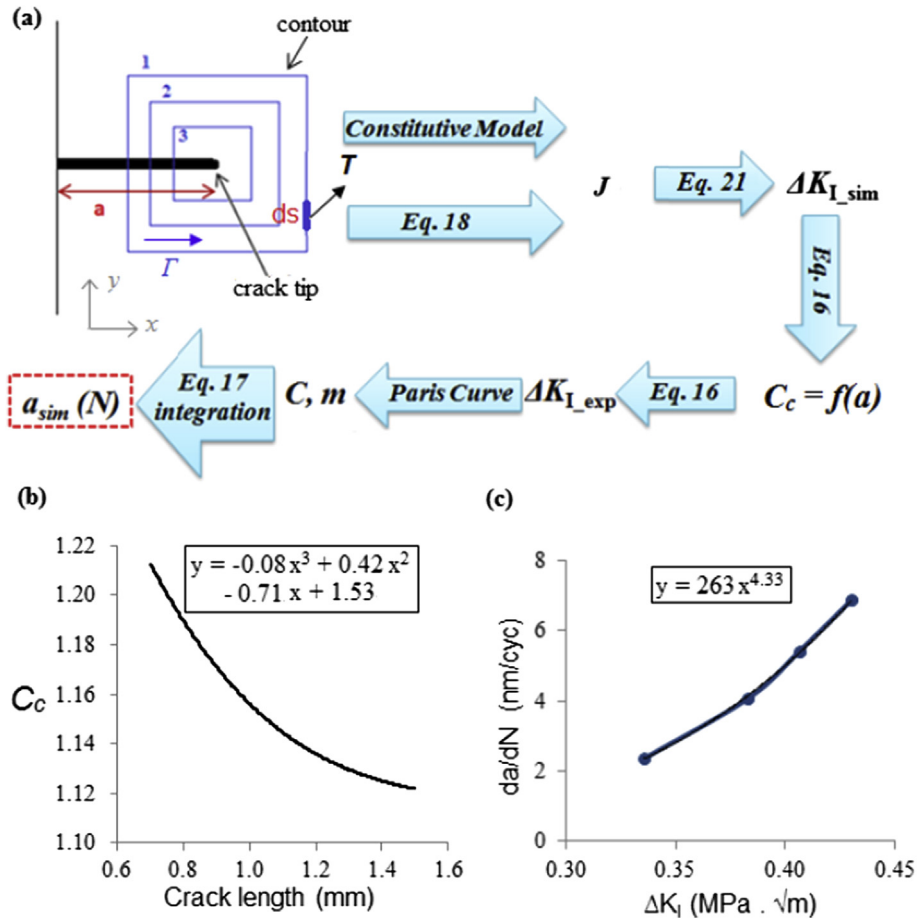

Fig. 6 – (a) Flowchart of the semi-analytical approach for crack propagation modelling; (b) configuration correction factor (C_c) versus crack length relationship at applied stress amplitude ($\Delta\sigma$) = 8.25 MPa; and (c) Paris curve for the membrane at 23 °C and 50% RH.

faces do not have any surface traction on them, the J-integral is path independent [53]. For isotropic linear elastic materials, the J-integral can be used to evaluate the stress intensity factor using the following relation

$$J = \frac{K_I^2}{E} \tag{21}$$

where E is the Young's modulus of elasticity.

Model description

The semi-analytical crack propagation model was implemented in MATLAB® to integrate the Paris law differential equation defined by Eq. (17). The Paris law parameters C and m, which are required to carry out this integration, were obtained by systematically utilizing: (i) the finite element method (FEM) based elastic-viscoplastic constitutive model presented in Sec. Elastic-viscoplastic constitutive model; (ii) the experimental data for crack propagation presented in Sec. Experimental results and discussion; and (iii) the analytical equations of fracture mechanics described in Sec. Theory. A flowchart of the semi-analytical approach is provided in Fig. 6a. The model simulates crack propagation by determining the crack length a as a function of the number of mechanical loading cycles N.

Because of symmetric conditions, only the left-half of the double edge crack specimen used during the experiments was modelled in COMSOL Multiphysics®. Three contours were drawn around the crack tip as shown in Fig. 6a. A total of 599 elements were used to mesh the geometry with high mesh density around the crack tip. Using the solution of the previously described elastic-viscoplastic constitutive model, the strain energy density W and traction vector T_i were determined at all points for all three contours. The J-integrals were then evaluated along each contour by integrating Eq. (18). Average values of J from the three contours were determined at both maximum and minimum applied stress states of the cyclic loading and were subsequently used to deduce the simulated cyclic variation of stress intensity factor ΔK_{I_sim} through Eq. (21). With $\Delta\sigma$ known from the loading conditions and ΔK_{I_sim} determined in the previous step, Eq. (16) was utilized to construct C_c versus crack length (a) curves for small incremental increases in crack length at different mechanical loading amplitudes and ambient (T, RH) conditions.

Assuming the C_c versus crack length relationship to be the same for both simulations and experiments, the experimental stress intensity factors ΔK_{I_exp} were calculated using Eq. (16). The average crack growth rates determined during the

experiments can now be plotted against ΔK_{I_exp} to generate the Paris curves. From the mathematical equation of the Paris curves, parameters C and m were deduced and thereafter, Eq. (17) was integrated from the initial crack length $a_i = 0.7$ mm to various incremental final crack length a_f values to evaluate the number of mechanical loading cycles (N) corresponding to each a_f value. Consequently, the simulated crack length (a_{sim}) could be obtained as a function of N. A reliable simulation of the crack propagation requires accurate construction of two intermediate characteristic curves: (i) the C_c versus crack length relationship; and (ii) the Paris curves. Fig. 6b and c shows examples of both for the membrane at 23 °C and 50% RH conditions along with the corresponding mathematical equations. The C_c was found to be a non-linearly decreasing function of the crack length that varies slightly with the applied stress level. For typical fatigue crack growth experiments conducted with double edge crack specimens under small-scale yielding conditions, the C_c versus crack length relationships can be found in standard mechanical testing handbooks such as ref. [54]. The C_c is generally not a function of specimen thickness. However, given that the experiments presented in this work were conducted on a very thin (25 μm) specimen wherein the specimen thickness can be comparable to the size of the plastic zone [14], these standard C_c versus crack length relationships may not be directly used for evaluating the ΔK_{I_exp} values needed for generating Paris curves from the experimental data. An indirect evaluation of ΔK_{I_exp} was therefore conducted here that involved the use of J-integrals obtained from the FEM-based constitutive model and generation of C_c versus crack length relationship specific to this problem, as illustrated in Fig. 6a. Paris curve shows the relationship between cyclic crack growth $\left(\frac{da}{dN}\right)$ measured in nm per cycle and the amplitude of the stress intensity factor ΔK_I measured in MPa.$\sqrt{m}$. The obtained Paris curve yielded the Paris law parameter values of $C = 263$ and $m = 4.33$ for the conditions specified here.

Model validation and discussion

Fig. 7 shows a comparison of experimentally measured and simulated crack propagation times for multiple test cases at four different combinations of temperature (23 °C and 70 °C) and RH (50% and 90%) conditions. In this comparison, the propagation time refers to the time taken (in hours) by a crack to increase from initial crack length a_i to final crack length a_f under the given conditions. The stress levels were varied during the test cases to capture results across a wide range of loading conditions. For graphical clarity, the stress amplitude on the horizontal axis in Fig. 7 is reversely categorical and not to scale. Within the experimental errors, which are typically large for fracture experiments, the propagation times predicted by considering elastic-viscoplastic material behaviour are in acceptable agreement with the experiments. The capability of the semi-analytical model to predict the *ex situ* crack propagation phenomenon in fuel cell membranes is thus validated for a range of temperature (23–70 °C) and humidity (50–90%) that is representative of fuel cell operation. Moreover, the Paris law approach was found to be effective in carrying out the fatigue-driven crack propagation analysis for this application. It should be noted that the present model is

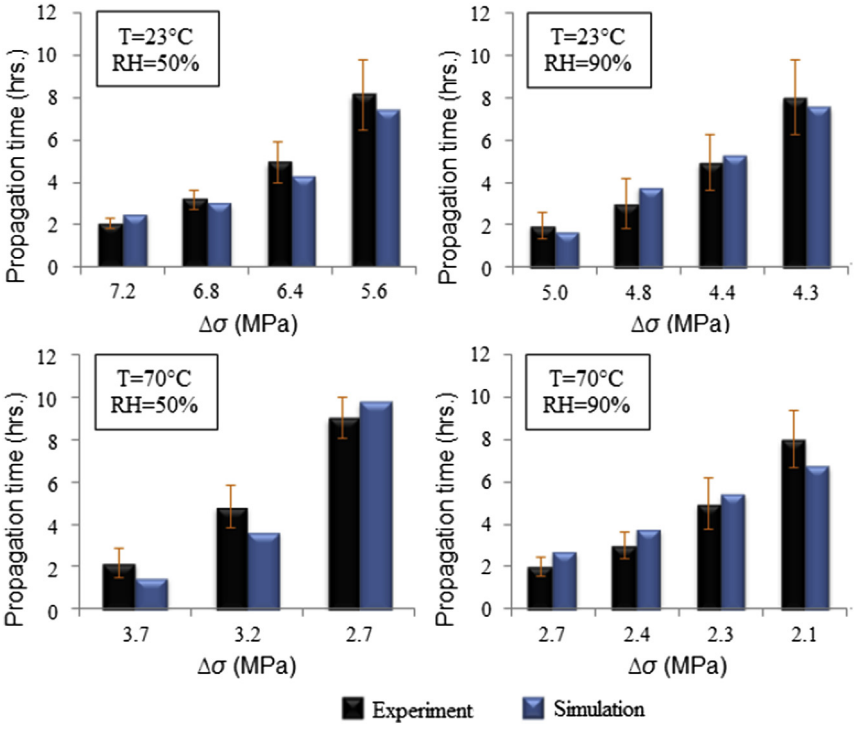

Fig. 7 – Comparison of experimental and simulated *ex situ* crack propagation time for membrane specimens at different stress amplitude $(\Delta\sigma)$, temperature (T), and RH conditions. For graphical clarity, the horizontal axis is reversely categorical and not to scale.

developed under an idealized plane-stress condition chosen to simulate the in-plane tensile tests conducted by Goulet et al. [8] and in-plane fracture tests discussed in Sec. Experimental investigation. In a practical case, both through-plane and in-plane membrane crack growth occurs in a fuel cell and most likely in that order leading to a gradual increase in crossover gas leakage. Given that the mechanical properties of the membrane are generally isotropic [45], the model is expected to be applicable to through-plane crack growth as well which can be idealized as plane-strain condition in fuel cells. This would, however, require an accurate simulation of dynamic *in situ* stresses that develop within fuel cell membranes during hygrothermal cycling which has been a subject of ongoing research [4,13,34,45]. Moreover, it is also clarified that the crack propagation modelling approach presented herein provides a one-dimensional result of crack length as a function of perpendicularly applied stress cycles and would not inherently capture the true directional characteristics of crack growth under *in situ* conditions wherein the stress fields can be three-dimensional. This limitation could, however, be overcome by considering the principal stresses to be the primary driver of *in situ* crack propagation analogous to the applied bulk stresses used during the experiments presented in Sec. Experimental investigation. The developed modelling framework thus provides a foundation for realising a complete fracture model for fuel cell membranes which could potentially become a useful simulation tool for fuel cell researchers and engineers to efficiently optimize membrane design under realistic working conditions.

A sensitivity analysis was also performed to investigate the effect of the material behaviour selection on the accuracy of the crack propagation simulations by replacing the elastic-viscoplastic constitutive behaviour in the FEM-based constitutive model with a linear elastic behaviour. The crack propagation time predicted from both material behaviour selections are compared in Fig. 8 along with the experimental results. At the standard conditions of 23 °C and 50% RH, both material behaviours were found to be reasonably accurate in predicting crack propagation. Notably, the elastic-viscoplastic treatment predicted somewhat faster crack growth because of larger plastic deformations and consequently larger surface area generation per cycle. When the RH was increased from 50% to 90%, the predictions from the linear elastic behaviour tended to deviate from the experimental results, whereas those from the elastic-viscoplastic behaviour still remained relatively accurate. This tendency was also observed at higher temperature (not shown here for brevity). These findings underline the criticality of incorporating elastic-viscoplastic material behaviour in order to obtain accurate crack propagation predictions particularly at the fuel cell operating conditions.

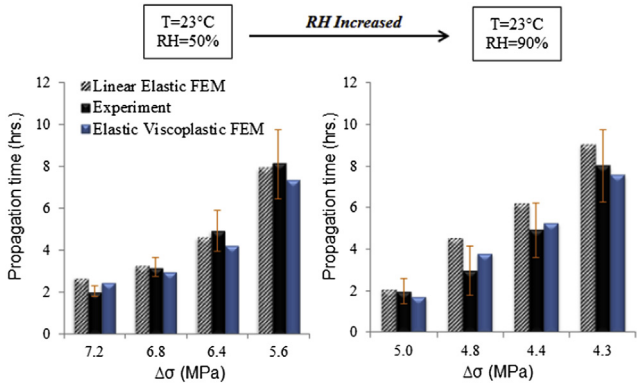

Fig. 8 – Effect of material behaviour selection on the accuracy of the crack propagation simulations.

Conclusions

A comprehensive *ex situ* experimental and modelling investigation was conducted in order to understand the fundamental nature of fatigue-driven crack propagation in automotive fuel cell membranes. Within the applied tensile stress range, the experimental results revealed that the crack growth rate in Nafion NRE211 membranes was typically ~1–10 nm per load cycle and increased relative to the applied stress, temperature, and humidity. Microstructural investigations of the fractured membrane specimens using three-dimensional X-ray computed tomography revealed localized plastic deformation around the fracture surface in the form of membrane thinning up to 60%. Moreover, the absence of plastic deformation in the bulk of the material confirmed that the crack propagation was driven by fatigue leading to a ductile fracture. A finite element based constitutive model was developed to simulate the elastic-viscoplastic mechanical response of fuel cell membranes during crack propagation. The *ex situ* simulations from the model not only compared well quantitatively with previously reported experimental results across a wide range of environmental conditions and strain rates, but were also able to effectively capture the typical qualitative characteristics of the mechanical response, *viz.* initial linear elasticity, gradual yielding, plastic strain with isotropic-hardening, and strain rate dependency.

The experimentally obtained correlations with stress, temperature, and humidity were utilized to develop a Paris law based semi-analytical model capable of predicting fatigue-driven crack propagation as a function of the number of load cycles when a crack-bearing membrane is subjected to cyclic mechanical loading. The finite element based elastic-viscoplastic constitutive model was integrated with the semi-analytical crack propagation model to accurately capture the ionomer membrane's complex mechanical response, while linear elastic fracture mechanics parameters were utilized based on the small-scale yielding observed during the experiments. The simulated results obtained with the semi-analytical crack propagation model were in acceptable agreement with the *ex situ* fracture experiments. The model was thereby validated for a range of stress, temperature, and humidity conditions relevant for fuel cell operation in automotive applications. Moreover, Paris law was found to be an effective approach for developing crack propagation tools based on empirical findings. It was also established that the elastic-viscoplastic treatment of ionomer membranes is necessary to accurately predict crack propagation across all relevant operating conditions, which highlights the importance of appropriate material behaviour selection during

fracture modelling of fuel cell membranes. The development of empirical crack propagation simulation capability within fuel cell membranes could be useful in efficient identification of practical mitigation strategies to tackle the critical failure mode of mechanical fracture, and therefore can potentially play a crucial role in improvement of fuel cell durability and their commercial viability in the automotive sector.

Acknowledgments

This research was supported by Ballard Power Systems and the Natural Sciences and Engineering Research Council (NSERC) of Canada through an Automotive Partnership Canada (APC) grant. We also acknowledge infrastructure funding provided by Canada Foundation for Innovation (CFI) and British Columbia Knowledge Development Fund (BCKDF). The research was undertaken, in part, thanks to funding from the Canada Research Chairs program. We thank Aronne Habisch for experimental assistance.

REFERENCES

[1] Garzon FH, Lau SH, Davey JR, Borup RL. Micro and nano X-Ray Tomography of PEM fuel cell membranes after transient operation. ECS Trans 2007;11:1139–49.
[2] Wu J, Yuan XZ, Martin JJ, Wang H, Zhang J, Shen J, et al. A review of PEM fuel cell durability: degradation mechanisms and mitigation strategies. J Power Sources 2008;184:104–19.
[3] Lai Y-H, Gittleman CS, Mittelsteadt CK, Dillard DA. Viscoelastic stress model and mechanical characterization of perfluorosulfonic acid (PFSA) polymer electrolyte membranes. 3rd Int Conf Fuel Cell Sci Eng Technol Ypsilanti 2005:161–7.
[4] Kusoglu A, Karlsson AM, Santare MH, Cleghorn S, Johnson WB. Mechanical response of fuel cell membranes subjected to a hygro-thermal cycle. J Power Sources 2006;161:987–96.
[5] Tang H, Peikang S, Jiang SP, Wang F, Pan M. A degradation study of nafion proton exchange membrane of PEM fuel cells. J Power Sources 2007;170:85–92.
[6] Aindow TT, O'Neill J. Use of mechanical tests to predict durability of polymer fuel cell membranes under humidity cycling. J Power Sources 2011;196:3851–4.
[7] Silberstein MN, Boyce MC. Constitutive modeling of the rate, temperature, and hydration dependent deformation response of Nafion to monotonic and cyclic loading. J Power Sources 2010;195:5692–706.
[8] Goulet MA, Khorasany RMH, De Torres C, Lauritzen M, Kjeang E, Wang GG, et al. Mechanical properties of catalyst coated membranes for fuel cells. J Power Sources 2013;234:38–47.
[9] Goulet M, Arbour S, Lauritzen M, Kjeang E. Water sorption and expansion of an ionomer membrane constrained by fuel cell electrodes. J Power Sources 2015;274:94–100.
[10] Pestrak M, Li Y, Case SW, Dillard D a, Ellis MW, Lai Y-H, et al. The effect of mechanical fatigue on the lifetimes of membrane electrode assemblies. J Fuel Cell Sci Technol 2010;7. 41009.
[11] Yan X, Hou M, Sun L, Cheng H, Hong Y, Liang D, et al. The study on transient characteristic of proton exchange membrane fuel cell stack during dynamic loading. J Power Sources 2007;163:966–70.
[12] Huang X, Solasi R, Zou YUE, Feshler M, Reifsnider K, Condit D, et al. Mechanical endurance of polymer electrolyte membrane and PEM fuel cell durability. J Polym Sci Part B Polym Phys 2006;44:2346–57.
[13] Lai Y-H, Mittelsteadt CK, Gittleman CS, Dillard DA. Viscoelastic stress analysis of constrained proton exchange membranes under humidity cycling. J Fuel Cell Sci Technol 2009;6. 21002.
[14] Kusoglu A, Santare MH, Karlsson AM. Aspects of fatigue failure mechanisms in polymer fuel cell membranes. J Polym Sci Part B Polym Phys 2011;49:1506–17.
[15] Khorasany RMH, Sadeghi Alavijeh A, Kjeang E, Wang GG, Rajapakse RKND. Mechanical degradation of PFSA membranes in polymer electrolyte membrane fuel cells under fatigue fracture tests. J Power Sources 2015;274:1208–16.
[16] Sadeghi Alavijeh A, Khorasany RMH, Habisch A, Wang GG, Kjeang E. Creep properties of catalyst coated membrane in polymer electrolyte fuel cells. J Power Sources 2015;285:16–28.
[17] Lim C, Ghassemzadeh L, Van Hove F, Lauritzen M, Kolodziej J, Wang GGG, et al. Membrane degradation during combined chemical and mechanical accelerated stress testing of polymer electrolyte fuel cells. J Power Sources 2014;257:102–10.
[18] Sadeghi Alavijeh A, Khorasany RMH, Goulet MA, Ghataurah J, Lauritzen M, Kjeang E, et al. Decay in mechanical properties of PEM fuel cell catalyst coated membranes subjected to accelerated stress testing. J Fuel Cells 2015;1:204–13.
[19] Wong KH, Kjeang E. Macroscopic in-situ modeling of chemical membrane degradation in polymer electrolyte fuel cells. J Electrochem Soc 2014;161:F823–32.
[20] Pozio A, Silva RF, De Francesco M, Giorgi L. Nafion degradation in PEFCs from end plate iron contamination. Electrochim Acta 2003;48:1543–9.
[21] Laconti A, Liu H, Mittelsteadt C, McDonald R. Polymer electrolyte membrane degradation mechanisms in fuel cells - findings over the past 30 Years and comparison with electrolyzers PEMFC membrane degradation mechanisms. ECS Trans 2006;1:199–219.
[22] Wong KH, Kjeang E. Mitigation of chemical membrane degradation in fuel cells: understanding the effect of cell voltage and iron ion redox cycle. ChemSusChem 2015;8:1072–82.
[23] Lim C, Sadeghi Alavijeh A, Lauritzen M, Kolodziej J, Knights S, Kjeang E. Fuel cell durability enhancement with cerium oxide under combined chemical and mechanical membrane degradation. ECS Electrochem Lett 2015;4:F29–31.
[24] Macauley N, Sadeghi Alavijeh A, Watson M, Kolodziej J, Knights S, Wang G, et al. Accelerated membrane durability testing of heavy duty fuel cells. J Electrochem Soc 2015;162:F98–107.
[25] Macauley N, Ghassemzadeh L, Lim C, Watson M, Kolodziej J, Lauritzen M, et al. Pt band formation enhances the stability of fuel cell membranes. ECS Electrochem Lett 2013;2:F33–5.
[26] Li Y, Quincy JK, Case SW, Ellis MW, Dillard DA, Lai Y. Characterizing the fracture resistance of proton exchange membranes. J Power Sources 2008;185:374–80.
[27] Patankar K, Dillard DA, Case SW, Ellis MW, Li Y, Lai Y. Characterizing fracture energy of proton exchange membranes using a knife slit test. J Polym Sci Part B Polym Chem 2010;48:333–43.
[28] Poornesh KK, Cho CD, Lee GB, Tak YS. Gradation of mechanical properties in gas diffusion electrode. Part 1: influence of nano-scale heterogeneity in catalyst layer on interfacial strength between catalyst layer and membrane. J Power Sources 2010;195:2718–30.
[29] Uchiyama T, Kato M, Ikogi Y, Yoshida T. Mechanical degradation mechanism of membrane electrode assemblies

in buckling test under humidity cycles. J Fuel Cell Sci Technol 2012;9. 61005.
[30] Uchiyama T, Kato M, Yoshida T. Buckling deformation of polymer electrolyte membrane and membrane electrode assembly under humidity cycles. J Power Sources 2012;206:37–46.
[31] Uchiyama T, Kumei H, Yoshida T. Catalyst layer cracks by buckling deformation of membrane electrode assemblies under humidity cycles and mitigation methods. J Power Sources 2013;238:403–12.
[32] Kai Y, Kitayama Y, Omiya M, Uchiyama T, Kato M. crack formation in membrane electrode assembly under static and cyclic loadings. J Fuel Cell Sci Technol 2013;10. 21007.
[33] Kai Y, Kitayama Y, Omiya M, Uchiyama T, Kumei H. In situ observation of deformation behavior of membrane electrode assembly under humidity cycles. J Fuel Cell Sci Technol 2014;11. 51006.
[34] Kusoglu A, Karlsson AM, Santare MH, Cleghorn S, Johnson WB. Mechanical behavior of fuel cell membranes under humidity cycles and effect of swelling anisotropy on the fatigue stresses. J Power Sources 2007;170:345–58.
[35] Khorasany RMH, Sadeghi Alavijeh A, Kjeang E, Wang GG, Rajapakse RKND. Simulation of ionomer membrane fatigue under mechanical and hygrothermal loading conditions. J Power Sources 2015;279:55–63.
[36] Khorasany RMH, Singh Y, Sadeghi Alavijeh A, Rajapakse RKND, Kjeang E. In-situ simulation of membrane fatigue in polymer electrolyte fuel cells. Int J Hydrog Energy 2017;42:11838–44.
[37] Banan R, Bazylak A, Zu J. Effect of mechanical vibrations on damage propagation in polymer electrolyte membrane fuel cells. Int J Hydrog Energy 2013;38:14764–72.
[38] Banan R, Zu J, Bazylak A. Humidity and temperature cycling effects on cracks and delaminations in PEMFCs. Fuel Cells 2015;15:327–36.
[39] Banan R, Bazylak A, Zu J. Combined effects of environmental vibrations and hygrothermal fatigue on mechanical damage in PEM fuel cells. Int J Hydrog Energy 2015;40:1911–22.
[40] Ding G, Santare MH, Karlsson AM. Numerical evaluation of fatigue crack growth in polymers based on plastically dissipated energy. Int J Fatigue 2017;94:89–96.
[41] Ding G, Santare MH, Karlsson AM, Kusoglu A. Numerical evaluation of crack growth in polymer electrolyte fuel cell membranes based on plastically dissipated energy. J Power Sources 2016;316:114–23.
[42] Khorasany RMH, Singh Y, Sadeghi Alavijeh A, Kjeang E, Wang GG, Rajapakse RKND. Fatigue properties of catalyst coated membranes for fuel cells: ex-situ measurements supported by numerical simulations. Int J Hydrogen Energy 2016;41:8992–9003.
[43] Sadeghi Alavijeh A, Venkatesan SV, Khorasany RMH, Kim WHJ, Kjeang E. Ex-situ tensile fatigue-creep testing: a powerful tool to simulate in-situ mechanical degradation in fuel cells. J Power Sources 2016;312:123–7.
[44] Paris PC, Gomez MP, Anderson WE. A rational analytic theory of fatigue. Trends Eng 1961;13:9–14.
[45] Khorasany RMH, Goulet MA, Sadeghi Alavijeh A, Kjeang E, Wang GG, Rajapakse RKND. On the constitutive relations for catalyst coated membrane applied to in-situ fuel cell modeling. J Power Sources 2014;252:176–88.
[46] Pommier S, Gravouil A. Extended finite element method for crack propagation. first ed. London, UK: ISTE; 2011.
[47] Singh Y, Orfino FP, Dutta M, Kjeang E. 3D visualization of membrane failures in fuel cells. J Power Sources 2017;345:1–11.
[48] Yoon W, Huang X. A nonlinear viscoelastic–viscoplastic constitutive model for ionomer membranes in polymer electrolyte membrane fuel cells. J Power Sources 2011;196:3933–41.
[49] Bergstrom JS, Boyce MC. Constitutive modeling of the large strain time-dependent behavior of elastomers. J Mech Phys Solids 1998;46:931–54.
[50] Bergström JS, Boyce MC. Large strain time-dependent behavior of filled elastomers. Mech Mater 2000;32:627–44.
[51] Joshi AY, Sharma SC, Harsha SP. Analysis of crack propagation in fixed-free single-walled carbon nanotube under tensile loading using XFEM. J Nanotechnol Eng Med 2010;1. 41008.
[52] Ragab A-R, Bayoumi SE. Engineering solid mechanics : fundamentals and applications. Boca Raton (FL), USA: CRC Press LLC; 1999.
[53] Rice JR. A path independent integral and the approximate analysis of strain concentration by notches and cracks. J Appl Mech 1968;35:379–86.
[54] Tada H, Paris PC, Irwin GR. The stress analysis of cracks handbook. second ed. Paris Productions & (Del Research Corp.); 1985.